Acta Mech 230:1441–1449 (2019)
https://doi.org/10.1007/s00707-017-2015-0

ORIGINAL PAPER

Hongti Zhang · Ka-Yu Fung · Yu Zhuang · Ke Cao · Jian Song · Alice Hu · Yang Lu

Fracture of a silicon nanowire at ultra-large elastic strain

Received: 5 June 2017 / Published online: 23 December 2017

Abstract Understanding the fracture behavior of one-dimensional (1-D) nanomaterials is critical for their functional device applications and maximizing their service life. At the nanoscale, solid materials' fracture properties could significantly deviate from their bulk counterparts. Our recent study (Zhang et al. in Sci. Adv. 2(8):e1501382, 2016. https://doi.org/10.1126/sciadv.1501382) showed that silicon (Si) nanowires, one of the most important functional 1-D nanomaterials for nanoelectronics and nano-electro-mechanical systems, demonstrated distinctly different mechanical properties than microscale and bulk Si crystals with the elastic strain up to 10% or even more, approaching their theoretical elastic limit. It is therefore intriguing to understand the fracture behavior of a Si nanowire under such deep ultra-strength, as well as their failure mechanisms. In this work, we will experimentally study the fracture behavior of ultrahigh elastic Si nanowires in situ and quantitatively understand their fracture mechanics with the assist of molecular dynamics simulations. The insights obtained in this nanomechanical study may be of help on the development of robust Si nanowire-based mechatronic devices.

1 Introduction

Fracture, the separation of material into two or more parts under stress, usually occurring due to the development of certain displacement discontinuity surfaces within the solid, is the common failure mechanism of materials under service. The study of materials' fracture behavior and the mechanism behind it is significant in guiding the design of industrial engineering materials to avoid failure and extend their service life [1]. Based on the intrinsic properties of materials, fracture can be divided into "brittle" and "ductile", two typical modes. For ductile fracture, the deformation strain is relatively large and with considerable plastic deformation (like thinning, necking, and elongation). For brittle fracture, the deformation strain is quite small due to the lack of plasticity, and the fracture surfaces are usually in flat or cleavage shapes [2].

Electronic supplementary material The online version of this article (https://doi.org/10.1007/s00707-017-2015-0) contains supplementary material, which is available to authorized users.

H. Zhang · K.-Y. Fung · Y. Zhuang · K. Cao · J. Song · A. Hu (✉) · Y. Lu (✉)
Department of Mechanical and Biomedical Engineering, City University of Hong Kong, Kowloon, Hong Kong, SAR, China
E-mail: alicehu@cityu.edu.hk

Y. Lu
E-mail: yanglu@cityu.edu.hk

H. Zhang · Y. Lu
Center for Advanced Structural Materials (CASM), Shenzhen Research Institute, City University of Hong Kong, Shenzhen 518057, China

Silicon, the most important electronic material in semiconductor industry, is known for rigid and brittle behavior at macroscale [3,4]. However, with sizes reduced into microscale, due to the size effect and related surface effect [5], silicon can become flexible [6,7]. Recently, we further discovered that a high-quality vapor–liquid–solid grown (VLS-grown) single-crystalline Si nanowire can have ultrahigh elasticity (>10%) before its fracture failure [8]. However, their fracture behavior at such ultra-large elastic strain remains unclear. In this work, the fracture behavior of Si nanowires at ultrahigh tensile elastic strain will be systematically examined based on our in situ SEM tensile testing platform starting from the examination of fracture surface morphology during and after tensile tests. With the assistance of numerical calculations and molecular dynamics (MD) simulations, surface roughness-induced local stress concentration and broken nanowire "flew away" phenomenon will be further discussed and explained. Roles of intrinsic crystalline defects like vacancies will also be put into consideration. This study can provide critical insights for the design and fabrication of Si nanowire-based electronic devices and nano-electro-mechanical systems (NEMS) to extend their service life.

2 Experimental results

The in situ SEM tensile tests of Si nanowires were performed based on a picoindenter-driven push-to-pull tensile testing platform [9] assisted with a micromechanical device (MMD) [10]. Upon the actuation of the picoindenter, the MMD can convert the indentation force from the indenter head into a tensile force on the sample stage, thus achieving the uniaxial tensile test on the clamped Si nanowires [11]. After reaching above 10% elastic deformation strain, the Si nanowires finally fractured, and the broken nanowires between the clamping points typically flew away after fracture [8].

As shown in Fig. 1, the fracture of the nanowires (at ∼ 13% elastic strain) occurred near the center part (Fig. 1b) and gradually disappeared under the relatively slow SEM scanning frames (Fig. 1c–e). Coming to the next frame, the remained nanowire "ghost" image (Fig. 1f) was also wiped away and left the empty devices with a tiny nanowire end on the clamping point (Fig. 1g). The corresponding stress versus strain curve of the Si nanowire was derived out from the raw force versus displacement data read from the picoindenter through a dedicated data conversion strategy [8] and is shown in Fig. 1h. The nanowire broke at the deformation strain of ∼ 13.1% with the stress of 16.1 GPa (calculated Young's modulus ∼ 123 GPa). During in situ testing, the Si nanowires experienced such an ultrahigh strain; however, the fracture process still appears in typical brittle manner, with a sudden failure without visible plastic deformation/necking. The nanowire flew away at the moment of fracture and cannot be captured by the SEM video due to the current SEM imaging recording speed limit. For example, in normal SEM operation, the real-time sample observation, the scanning rate is typically set at 300 ns for a 768 × 512 resolution, so each frame of picture costs ∼ 146.5 ms—within the time

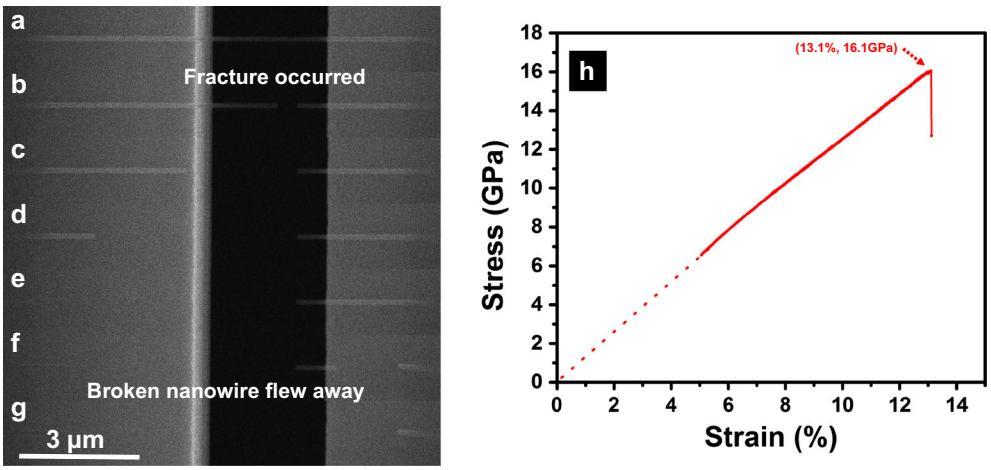

Fig. 1 Fracture process of a VLS-grown single-crystalline silicon (Si) nanowire during in situ SEM tensile testing: **a** the ultrahigh elastic Si nanowires at the moment right before fracture; **b–e** the broken nanowire retracts and disappears ("flew away") upon "re-bounce"; **f** the residual nanowire ghost image due to slow SEM scanning speed; **g** the left Si nanowire at the bonding part; **h** the corresponding stress versus strain curve of the tested VLS Si nanowire

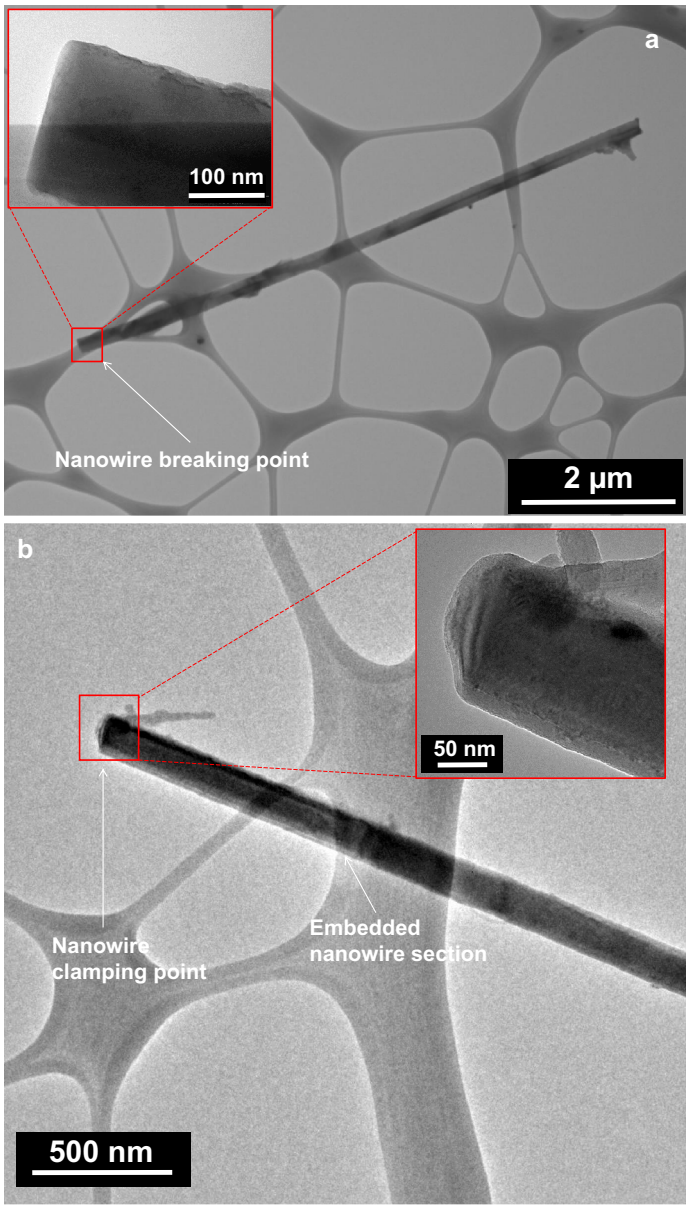

Fig. 2 Postmortem TEM images of the ultrahigh elastic Si nanowires for its fracture surface (**a**) and the fracture surfaces near the clamping area (**b**) due to the secondary breaking at the clamping part. The zoomed views on the fracture surfaces are shown in each inserted red frames

of taking 1 full frame of SEM scanning, the broken nanowires already flew away, and we cannot capture the whole failure process.

Then, the postmortem TEM analysis was used to examine the broken Si nanowires after successfully picking the remaining nanowire parts near the clamping points (sometimes, the half broken nanowire was remaining, as shown in Ref. [8]). As shown in Fig. 2a, the fracture surface where the fracture starts is flat for the sample after experiencing more than 10% of elastic deformation. While for another case presented in Fig. 2b, we examined the fracture surface of the remaining nanowire section near the clamping point—which is more typical for most postmortem TEM sample images, which was believed because the broken nanowire had experienced secondary fracture near the clamping area, after large elastic strain energy was released upon the first fracture event. However, the detailed mechanism requires MD simulations to interpret (as follows).

3 Analysis and discussion

3.1 Ultrahigh elastic strain energy

To understand the "flying away" phenomenon of Si nanowires upon fracture, the accumulated elastic strain energy during deformation inside the nanowire was firstly calculated based on the ~ 13% elastic strain before fracture. Based on the classic elasticity theory and equations derived from Landau's Theory of Elasticity [12], the elastic potential energy at this elastic strain value can be calculated as follows:

$$U_{\mathrm{e}} = \int \frac{Y A_0 \Delta l}{l_0} dl = \frac{Y A_0 \Delta l^2}{2 l_0}$$

Here,
Y: Young's modulus of the material;
A_0, cross-sectional area;
l_0, initial length;
Δl, stretched length.

In our case,

Y: ~ 123 GPa (can be varied due to the size effect; here, the value was calculated based on our stress-strain measurements);
A_0: $\sim 5.805 \times 10^{-15} \mathrm{m}^2$;
l_0: 5.86×10^{-6} m;
Δl: 0.78×10^{-3} m.

Then, the calculated elastic strain energy will be

$$U_{\mathrm{e}} = 3.71 \times 10^{-11} J = 2.32 \times 10^{8} \mathrm{eV},$$

which is equal to 1/7 of the volumetric energy density of TNT (2,4,6-trinitrotoluebe) [8].

Assuming the conversion rate of elastic potential energy into kinetic energy is 100% (of course, the real conversion rate should be less than 100%, due to the other forms of energy consumption and residual energy, such as surface energy and residual defect energy), at this energy level, the generated velocity on each Si atom at the fracture moment was calculated as follows [13]:

$$U_{\mathrm{e}} = U_k = \frac{1}{2} \mathrm{m} \mathrm{v}^2,$$

$$v = \sqrt{\frac{2U_{\mathrm{e}}}{m}}.$$

Putting the potential energy of $\sim 0.22 \times 10^{-19}$ J (which is derived based on the original size of the Si nanowire of $A_0 \times l_0 = 34 \times 10^{-15}$ cm^3) and mass weight of $\sim 4.65 \times 10^{-23}$ for each Si atom into the above equation, the calculated velocity of the Si nanowire upon fracture is ~ 970 m/s, which is nearly three times of the sound speed (acoustic wave in the air) at room temperature of ~ 330 m/s. This further supports that capturing the detailed fracture process of a Si nanowire frame by frame is virtually impossible based on the current SEM imaging technique.

On the other hand, with that high velocity, the broken nanowires retract/bounce back ("rebound") instantly and will be stopped by the bonding glue. Then, a reaction force on the clamping part will be generated and causes the secondary fracture as well as the following broken nanowire "flew away" phenomenon. The rebound force at that time is complicated and could be mixed with compression, bending, shearing loads. However, existing imaging technique cannot capture these details, which requires modeling to reproduce this phenomenon.

3.2 MD simulation on the multi-step fracture of a Si nanowire under large elastic strain

In order to reproduce and in-depth understand the multiple nanowire fracture events and associated broken nanowires "flew away" phenomenon [8], we further performed molecular dynamics (MD) simulations by using LAMMPS [14]. As shown in Fig. 3, we built up a Si nanowire model with of 5780 Si atoms, 20 Å in

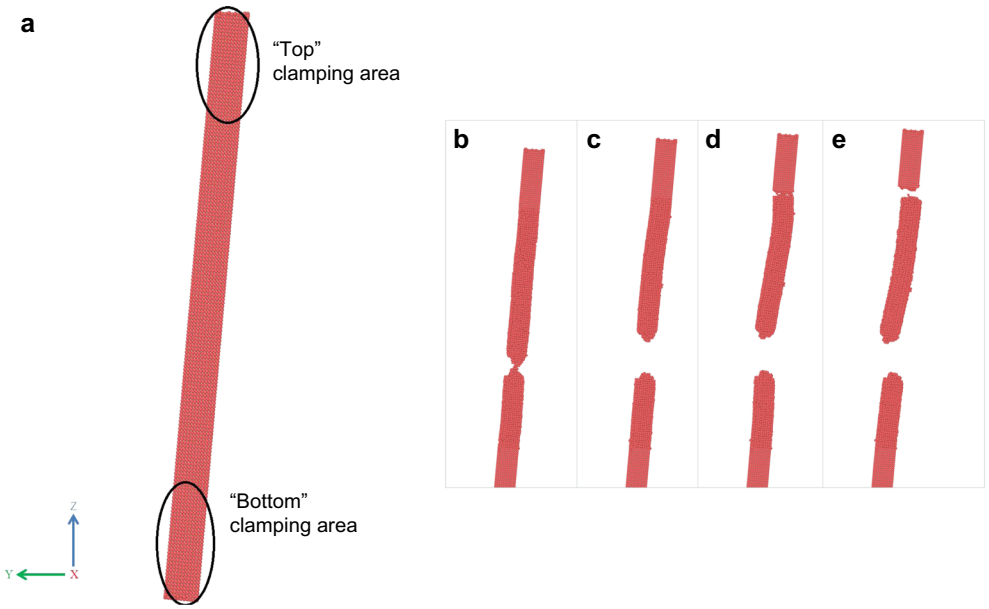

Fig. 3 Molecular dynamics (MD) simulations of the multi-step fracture process of a Si nanowire: **a** model construction and boundary setup; **b**, **c** fracture process at the first breaking; **d**, **e** fracture process during the secondary breaking, which led to the broken nanowire pieces' "flying away" phenomenon, as observed in most experiments

diameter and 358 Å in length with the fixed boundary conditions to simulate the clamping point condition. In order to prevent a loss of atoms during tension simulation, the simulation box is 2000 Å in *X*, *Y*, and *Z* dimensions, which is much larger than the nanowire geometry. The spline-based modified embedded atom method (Si_2.MEAM/spline) pairing potential [15,16] is used in the MD simulations. An NVE (the constant thermal energy and volume time integration) is used in carrying out the modeling, and the temperature was set at 300K. The time step of simulation is 0.01 ps.

In order to reproduce the actual bonding condition of our nanowire samples, the top and bottom 60 Å of the nanowire model are set as the clamping areas "top" and "bottom" (see Fig. 3a). Atoms' force in "top" and "bottom" is set to zero by the "setforce" command. 1 Å /ps velocity is imposed to atoms in the "top" region, imitating the pulling (tension) of the nanowire. The direction of this velocity is parallel to the axis of the wire. For simplicity, only one tail is pulled in this simulation, and a high "pulling velocity" is used for reducing computation time. The "pulling velocity" is kept constant until the end of simulation because the pulling will not stop precisely at the moment of breaking of the nanowire in experiment. Once the wire is broken, a reflection wall is set at the bottom of "top," which acts like a massive wall reflecting atoms moving upward from below by elastic collision ("rebound"). Due to the fact that typical clamping may not be perfect, slightly tilting of the clamping condition was considered, so the wire is slightly tilted to -*Y* direction for 5° while the reflection wall is set to be a horizontal plane, relative to the simulation box, at the *Z* coordinates of the most bottom atoms of "top."

The results shown in Fig. 3b indicate the moment just before the first fracture, while the first fracture (also the main fracture of the Si nanowire) is shown in Fig. 3c. Upon the releasing of stored large elastic energy, the broken nanowire bounced back, with ultra-fast velocity, three times of the sound speed, hit the bonding point (clamping area). Then, Fig. 3d shows that the secondary fracture occurred near the clamping area, due to the "bounce back" of the broken nanowire after first breaking. With the mixed loading conditions including bending, shearing, compression, and re-bounce, the broken nanowire section experienced a secondary fracture, as shown in Fig. 3e, with a complete detachment of the remaining wire near the clamping area (see Supplementary Video S1 for the whole process of the multi-step fracture), leading to the final "flying away" phenomenon.

3.3 Inhibition of plasticity before facture

To achieve such high elasticity in Si nanowires, the foremost issue is the inhibition of the onset of plasticity in the Si nanowire during large elastic deformation. However, for a pristine Si macrostructure without visible

defects, the dislocations inside it would be expected to be injected from the source under deformation, then pile up and tangle with the deformation continuing. And finally form a weak point by accumulation of abundant dislocations to initiate a crack. The following crack initiation process will lead the Si microstructure to fracture. For a Si structure at microscaling, it has been observed that the nucleation of dislocations at the surface can finally cause mechanical failure, which normally involves the interactions of multiple dislocations and the following pileups of immobile dislocations. When we come to Si nanowires with diameters down to $\sim$ 100 nm, it is still possible to have a similar dislocation nucleation and pileup behavior that cause the weak point formation and lead to final fracture. However, as presented by the high-resolution TEM images of our ultrahigh elastic Si nanowires [8], in our VLS-grown Si nanowires with pristine single-crystalline structure, defects like preexisting dislocation and grain boundary will not be a major issue. Even voids generated by the formation and accumulation of vacancy may not be sufficient enough to cause plasticity, as estimated: based on traditional theories, the vacancy formation energy for a high-purity silicon was determined to be about 4.0 eV [17,18]. While in our case, the calculated potential energy of each Si atom at $\sim$ 13% elastic deformation strain is 0.136 eV by distributing the total 2.32×10^8 eV onto all atoms participating at the deformation, which is far below the vacancy formation energy. The total atoms participating deformation process is calculated as follows [19]:

$$N = \frac{\rho \times A_0 \times l_0}{M} \times \mathrm{N_A}.$$

Here,
ρ, density of Si at room temperature, 2.33 g cm^{-3} [20];
A_0, cross-sectional area, 5.805×10^{-15}m^2;
l_0, initial length, 5.86×10^{-6} m;
M, molar mass of Si, 28 g mol^{-1};
N_A, Avogadro constant, 6.02×10^{23} mol^{-1}.

Putting the parameters into the equation, finally we get:

$$N = 1.7 \times 10^9.$$

The vacancy concentration of Si nanowires can be calculated as follows [21,22]:

$$C_0 = N_0 \exp\left(\frac{-E^f}{k_B T}\right) = \frac{\rho N_A}{M} \exp\left(\frac{-E^f}{k_B T}\right).$$

Here,
N_0, total number of atoms per unit volume;
ρ, density of Si at room temperature, 2.33 g cm^{-3};
N_A, Avogadro constant, 6.02×10^{23} mol^{-1};
M, molar mass of Si, 28 g mol^{-1};
E^f, formation energy of a neutral vacancy;
k_B, Boltzmann constant;
T, temperature.

After calculation, we get the vacancy concentration in the Si nanowires which is $\sim 8.89 \times 10^{-46}$ cm^{-3}, which is extremely low and cannot contribute to the nucleation of voids and form major defects. Therefore, the onset of plasticity during elastic deformation of Si nanowires can be effectively inhibited by the lack of crystalline defects (such as dislocation or nucleated vacancies) as well as the easy escape of the defects from the surface due to the ultra-small volume.

3.4 Inhibition of premature fracture

Beside plasticity, another key aspect to make sure Si nanowires which can be stretched up to such a large elasticity is "without premature fracture." In this scenario, the surface roughness of the Si nanowire is apparently a critical issue [5,23]. For a Si macrostructure at bulk or microscales, it will break in brittle manner upon applied tensile strain with the crack propagation mechanism [24]. Even though the crack initiation and following propagation process is complicated, finally, the fracture surface is neat and clean which typifies the brittle fracture (as shown in Fig. 2a). According to the classical Griffith theory as presented below, there will be a

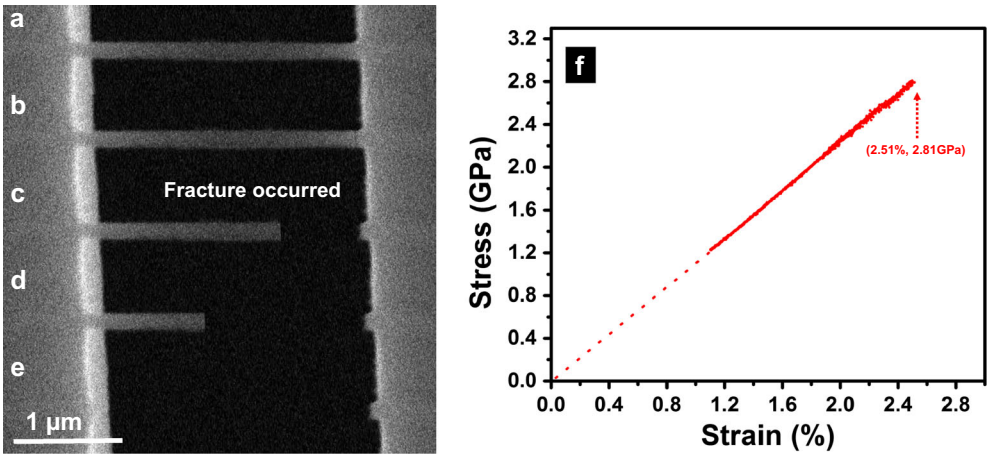

Fig. 4 Fracture process of a top–down etched Si nanowire with ~ 4% elasticity recorded by SEM. **a** Si nanowire right before fracture; **b–d** disappearing process of the brittle broken Si nanowire part; **e** the left Si nanowire near the bonding part; **f** the corresponding stress versus strain curve of the tested top-down etched Si nanowire

significant stress concentration at the crack tip which is much larger than the applied stress and enough to drive the crack propagation at certain roughness places [24]:

$$\sigma_m = 2\sigma_0\sqrt{\frac{a}{\rho_t}} = K_t\sigma_0.$$

Here,
σ_m, stress at the crack tip;
σ_0, applied stress;
ρ_t, radius of curvature;
K_t, stress concentration factor [25].

Again, as presented by the high-resolution TEM images of the ultrahigh elastic Si nanowires, the surface of the VLS-grown nanowires is almost atomically scale smooth [8]; thus, the influence of the surface roughness' caused stress concentration is negligible for the ultrahigh elasticity nanowires.

For comparison, the fracture behavior of top–down etched Si nanowires which was featured with a relatively rougher surface was studied likewise. Based on the Griffith theory, the existence of those surface roughnesses would be effectively like half-cracks on the surface, which lead to local stress concentration and cause $Kt > 1$. Even the applied global stress σ_0 is small, but at the roughness kinked sites/half-crack, the induced local stress σ_m will be much larger and reaches the theoretical maximum fracture stress of Si, thus leading to the fracture of Si at roughness places. The further crack propagation will lead the Si crystals typically to break ahead of their theoretical strength. Consequently, the maximum fracture strains were ~ 2.5% for the top–down etched Si nanowires [8], far below the theoretical elastic deformation strain of ~ 17%, and the deformation strain of VLS-grown atomic smooth counterparts of ~ 13%. The fracture process recorded in SEM is shown in Fig. 4. As presented in the image frames of Fig. 4b, the fracture starts near one and ends near the stage edge, and then, the broken nanowire further disappears in a tempo sequence as presented in Fig. 4c, d (still, due to the relatively slow scanning speed of SEM). In Fig. 4e, the fracture surface on the remaining part was non-uniform. The calculated stress versus strain curve records that the nanowire deformation is still linear, which indicates that the deformation process of the Si nanowire is elastic even though at a much lower fracture stress of ~ 2.81GPa and strain of ~ 2.51% (calculated Young's modulus is ~ 112 GPa), which is much lower than the VLS-grown one due to the premature fracture. This further supported that the fracture process of the top–down etched Si nanowires follows the crack initiation and propagation process due to the surface roughness [24], but the fracture is in typical brittle feature.

4 Conclusions

By experimental nanomechanical characterization and theoretical calculations, the fracture behaviors of Si nanowires at ultrahigh elastic strains were systematically studied. From in situ SEM imaging of the fracture

process, we observed that Si nanowires, even with such high elastic deformation strain, still broke in a brittle manner: postmortem TEM analysis of the fracture surface showed brittle-like flat surfaces while MD simulations confirmed the multi-step process of the fractured nanowires, causing that the broken pieces typically "flew away." A further analysis showed that the ultra-low intrinsic defect concentrations in the high-quality VLS-grown Si nanowire crystals reduced the accumulation of defects, thus inhibited the plasticity. Meanwhile, the atomic-level smooth surface morphology prevented the premature fracture by surface cracks/roughness. This research shows a new type of fracture behavior of Si crystals in which brittle fracture still dominates the failure but ultra-large (elastic) strain can be achieved prior to the fracture. This work could provide valuable insights for the design and fabrication of next-generation flexible electronics [26] or bio-nano-integrated systems [27] based on Si or other semiconductor nanowires with such deep ultra-strength.

Acknowledgements The authors gratefully thank Prof. KN Tu (UCLA), Dr. J. Tersoff (IBM) and Prof. J. Li (MIT) for the valuable discussions on this work. This research was supported by the Research Grants Council of the Hong Kong Special Administrative Region, China, under the projects CityU 138813 and CityU 11216515 and the National Natural Science Foundation of China (NSFC) Grant 51301147. A.H. acknowledges the funding support from City University of Hong Kong under the Project 9610336.

References

1. Kang, K., Cai, W.: Brittle and ductile fracture of semiconductor nanowires–molecular dynamics simulations. Philos. Mag. **87**(14–15), 2169–2189 (2007). https://doi.org/10.1080/14786430701222739
2. Lu, Y., Song, J., Huang, J.Y., Lou, J.: Fracture of sub-20 nm ultrathin gold nanowires. Adv. Funct. Mater. **21**(20), 3982–3989 (2011). https://doi.org/10.1002/adfm.201101224
3. DelRio, F.W., Cook, R.F., Boyce, B.L.: Fracture strength of micro- and nano-scale silicon components. Appl. Phys. Rev. **2**(2), 021303 (2015). https://doi.org/10.1063/1.4919540
4. Wang, Y., Xie, D., Ning, X., Shan, Z.: Thermal treatment-induced ductile-to-brittle transition of submicron-sized Si pillars fabricated by focused ion beam. Appl. Phys. Lett. **106**(8), 081905 (2015). https://doi.org/10.1063/1.4913241
5. Eremeyev, V.A.: On effective properties of materials at the nano-and microscales considering surface effects. Acta Mech. **227**(1), 29–42 (2016)
6. Zhu, Y., Xu, F., Qin, Q., Fung, W.Y., Lu, W.: Mechanical properties of vapor–liquid–solid synthesized silicon nanowires. Nano Lett. **9**(11), 3934–3939 (2009). https://doi.org/10.1021/nl902132w
7. Dongfeng, Z., Breguet, J.-M., Clavel, R., Sivakov, V., Christiansen, S., Michler, J.: In situ electron microscopy mechanical testing of silicon nanowires using electrostatically actuated tensile stages. J. Microelectromech. Syst. **19**(3), 663–674 (2010). https://doi.org/10.1109/jmems.2010.2044746
8. Zhang, H., Tersoff, J., Xu, S., Chen, H., Zhang, Q., Zhang, K., Yang, Y., Lee, C.-S., Tu, K.-N., Li, J., Lu, Y.: Approaching the ideal elastic strain limit in silicon nanowires. Sci. Adv. **2**(8), e1501382 (2016). https://doi.org/10.1126/sciadv.1501382
9. Zhang, H., Jiang, C., Lu, Y. (2016) Low-cycle fatigue testing of Ni nanowires based on a micro-mechanical device. Exp. Mech. https://doi.org/10.1007/s11340-016-0199-1
10. Lu, Y., Ganesan, Y., Lou, J.: A multi-step method for in situ mechanical characterization of 1-D nanostructures using a novel micromechanical device. Exp. Mech. **50**(1), 47–54 (2010). https://doi.org/10.1007/s11340-009-9222-0
11. Ganesan, Y., Lu, Y., Peng, C., Lu, H., Ballarini, R., Lou, J.: Development and application of a novel microfabricated device for the in situ tensile testing of 1-D nanomaterials. J. Microelectromech. Syst. **19**(3), 675–682 (2010). https://doi.org/10.1109/Jmems.2010.2046014
12. Landau, L.D., Lifshitz, E.M.: Theory of Elasticity, 3rd edn. Butterworth Heinemann, Oxford (1986)
13. Jain, M.C.: Textbook of Engineering Physics (Part I). PHI Learning Private Limited, New Delhi (2009)
14. Plimpton, S.: Fast parallel algorithms for short-range molecular dynamics. J. Comput. Phys. **117**(1), 1–19 (1995)
15. Lenosky, T.J., Sadigh, B., Alonso, E., Bulatov, V.V., de la Rubia, T.D., Kim, J., Voter, A.F., Kress, J.D.: Highly optimized empirical potential model of silicon. Modell. Simul. Mater. Sci. Eng. **8**(6), 825 (2000)
16. Du, Y.A., Lenosky, T.J., Hennig, R.G., Goedecker, S., Wilkins, J.W.: Energy landscape of silicon tetra-interstitials using an optimized classical potential. Phys. Status Solidi (b) **248**(9), 205–2055 (2011)
17. Fukata, N., Kasuya, A., Suezawa, M.: Formation energy of vacancy in silicon determined by a new quenching method. Phys. B Condens. Matter **308–310**, 1125–1128 (2001). https://doi.org/10.1016/S0921-4526(01)00908-5
18. Fukata, N., Kasuya, A., Suezawa, M.: Vacancy formation energy of silicon determined by a new quenching method. Jpn. J. Appl. Phys. **40**(8B), L854 (2001)
19. Sanders, I.R., Dobson, P.S.: Oxidation, defects and vacancy diffusion in silicon. Philos. Mag. **20**(167), 881–893 (1969). https://doi.org/10.1080/14786436908228058
20. Hull, R.: Properties of Crystalline Silicon, vol. 20. IET, London (1999)
21. Saito, M., Ohno, T., Yamasaki, T.: Density-functional-theory-based calculations of formation energy and concentration of the silicon monovacancy. Jpn. J. Appl. Phys. **54**(4), 041301 (2015)
22. Dannefaer, S., Mascher, P., Kerr, D.: Monovacancy formation enthalpy in silicon. Phys. Rev. Lett. **56**(20), 2195–2198 (1986)
23. Liu, Q., Wang, L., Shen, S.: Effect of surface roughness on elastic limit of silicon nanowires. Comput. Mater. Sci. **101**, 267–274 (2015)
24. Schiavone, A., Abeygunawardana-Arachchige, G., Silberschmidt, V.V.: Crack initiation and propagation in ductile specimens with notches: experimental and numerical study. Acta Mech. **227**(1), 203–215 (2016)
25. Griffith, A.A.: The phenomena of rupture and flow in solids. Philos. Trans. R. Soc. Lond. Ser. A Contain. Pap. Math. Phys. Character **221**(582—-593), 163–198 (1921). https://doi.org/10.1098/rsta.1921.0006

26. Xu, S., Yan, Z., Jang, K.-I., Huang, W., Fu, H., Kim, J., Wei, Z., Flavin, M., McCracken, J., Wang, R., Badea, A., Liu, Y., Xiao, D., Zhou, G., Lee, J., Chung, H.U., Cheng, H., Ren, W., Banks, A., Li, X., Paik, U., Nuzzo, R.G., Huang, Y., Zhang, Y., Rogers, J.A.: Assembly of micro/nanomaterials into complex, three-dimensional architectures by compressive buckling. Science **347**(6218), 154–159 (2015). https://doi.org/10.1126/science.1260960
27. Tian, B., Liu, J., Dvir, T., Jin, L., Tsui, J.H., Qing, Q., Suo, Z., Langer, R., Kohane, D.S., Lieber, C.M.: Macroporous nanowire nanoelectronic scaffolds for synthetic tissues. Nat. Mater. **11**(11), 986–994 (2012). https://doi.org/10.1038/nmat3404